# Scaling up a hollow fibre reactor: A study on non-PGM hollow fibre after-treatments for methane emission control under extreme conditions

Miguel García-Vázquez [a], Pablo Marín [b], Salvador Ordóñez [b], Kang Li [c], Jinkun Tan [d], Guangru Zhang [d] and Francisco R. García-García [a*]

[a]*School of Engineering, Institute for Materials and Processes, University of Edinburgh, Robert Stevenson Road, Edinburgh EH9 3FB, UK*

[b]*Catalysis, Reactors and Control Research Group (CRC), Department of Chemical and Environmental Engineering, University of Oviedo, Oviedo 33006, Spain*

[c]*Barrer Centre, Department of Chemical Engineering, Imperial College London, Exhibition Road, London SW7 2AZ, United Kingdom*

[d]*State Key Laboratory of Materials-Oriented Chemical Engineering, College of Chemical Engineering, Nanjing Tech University, 30 Puzhu Road(S), Nanjing 211816, P.R. China*

**Corresponding author: francisco.garcia-garcia@ed.ac.uk*

## Abstract

Hollow fibre-based after-treatments impregnated with iron and chromium-based oxides (non-PGM) have been tested for residual methane catalytic oxidation under extreme conditions (sulfur concentration 100-times larger than in real conditions), real timeframes (1000 h) and real operating cycles (thermal shocks). The results from this study have proven, for the first time reported in the literature, that hollow fibre reactors can be scaled up and that non-PGM impregnated hollow fibre after-treatments are the ideal candidate for the development of commercial residual methane after-treatments.

## Keywords

Natural Gas, Methane Emission Control, Hollow Fibre After-treatment, non-PGM catalysts, sulfur-resistant catalysts

## 1. Introduction

Global consumption of natural gas is increasing every year. In 2019, it grew by 2.6% and 3,986 billion cubic metres of natural gas were consumed [1], a volume 50% larger than the water volume of Lake Victoria in East Africa. Moreover, with proven natural gas reserves of over 200,000 billion cubic metres [1], or ten times the water volume of the Baltic Sea in Northern Europe, natural gas will be the most consumed fossil fuel by 2050.

Natural gas is regarded as a bridge fuel since its combustion produces 50% less carbon dioxide than that of coal and 30% less than that of oil [2,3]. However, natural gas is a mixture of hydrocarbons made up of over 90% methane, itself a greenhouse gas with a 20-year global warming potential of 84 [4]. It is reported that natural gas power plants emit concentrations of up to 1400 ppmV of non-combusted methane [5]. Although these concentration levels may seem negligible, they should not be left untreated. At a concentration of 5000 ppmV of non-combusted methane, the environmental impact of natural gas technologies is comparable to that of oil. At even higher concentrations of 1% of non-combusted methane, technologies fuelled by methane are dirtier than coal. There is currently no commercially available technology for treating residual methane emissions. Therefore, if natural gas is to be the bridge between fossil fuels and renewables, effective and affordable methods of controlling these methane emissions must be developed. Until then, these emissions will remain unregulated and overlooked.

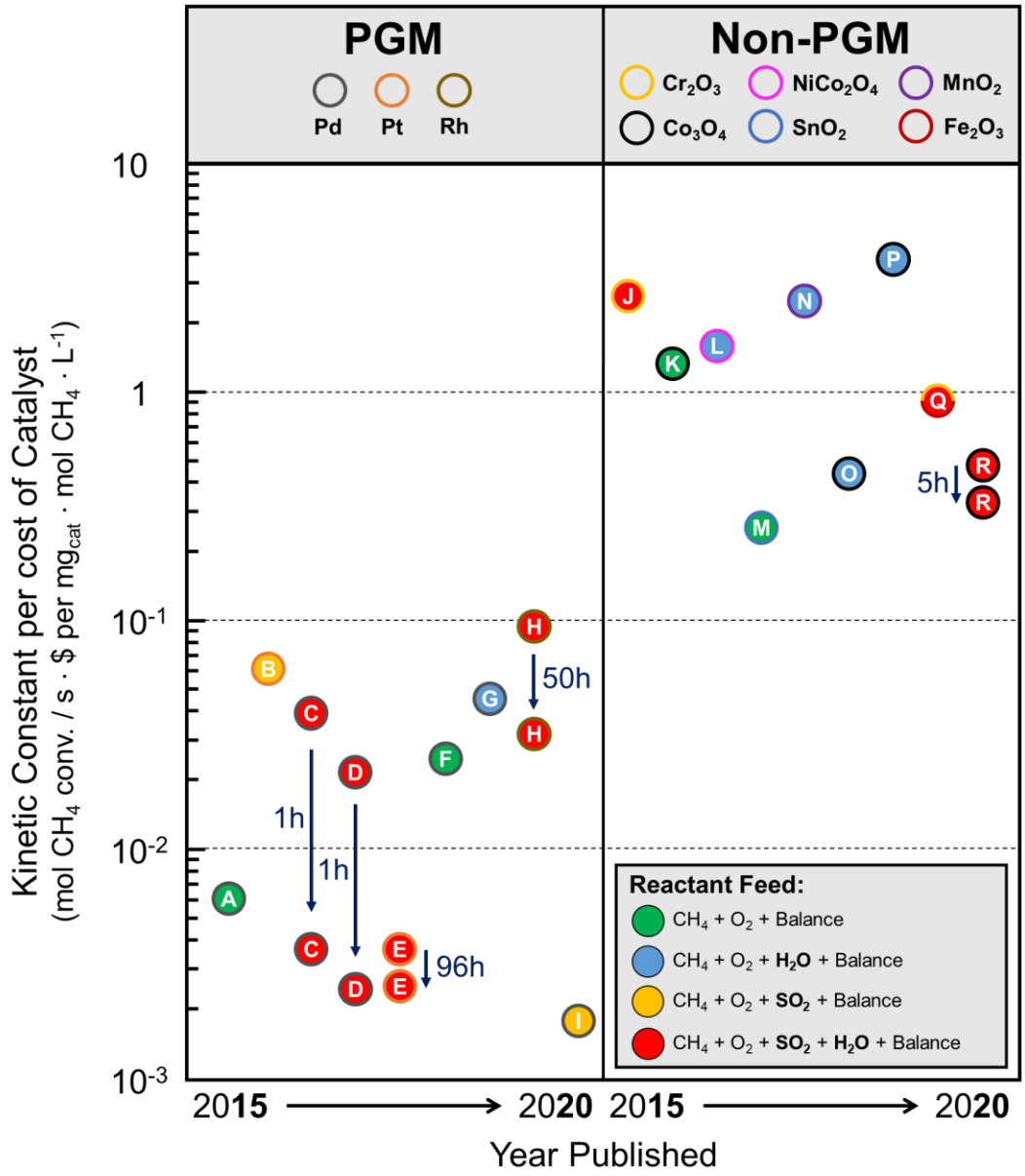


*Fig. 1: Cost-effectiveness analysis of the main catalysts studied over the past 5 years. Ref – PGM: A* [6], *B* [7], *C* [8], *D* [9], *E* [10], *F* [11], *G* [12], *H* [13] *and I* [14]. *Non-PGM: J* [15], *K* [16], *L* [17], *M* [18], *N* [19], *O* [20], *P* [21], *Q* [22] *and R* [23]. *The bulk metal prices that have been used to calculate the kinetic constant per cost of catalyst are the following: PGM: Pd (94.20 $/g), Pt (39.45 $/g), Rh (19.29 $/g) – Non-PGM: $Cr_2O_3$ (4.50 $/Kg), NiO (12.86 $/Kg), $MnO_2$ (10.00 $/Kg), $Co_3O_4$ (7.71 $/Kg), $SnO_2$ (32.10 $/Kg) and $Fe_2O_3$ (1.40 $/Kg). References can be found in Table S1 in the supplementary information.*

Catalytic oxidation is the most favoured methane abatement technology due to its environmental and economic advantages [15,24]. A selection of the most relevant methane oxidation catalysts studied between 2015 and 2020 have been presented in Fig. 1. As can be seen, two types of catalysts are currently used for the total oxidation of residual methane: platinum group metals (PGM) [6–14] and non-platinum group metals (non-PGM) [15–23]. The data shown in Fig. 1 shows the kinetic constant per cost of catalyst, which has been calculated using the total flowrate, the methane feed concentration, the reaction conversion, the mass of active phase of catalyst and the bulk cost of the main metals present in each catalyst. When cost is taken into consideration, PGM catalysts cannot compete with non-PGM catalysts. In addition, under real conditions including sulfur dioxide, arising from non-removed hydrogen sulfide and/or sulfur-containing odorants, as well as steam among the reactants, the deactivation of PGM-based catalyst results in a drastic loss of activity. The single most important factor for the development of effective residual methane emission catalytic systems is overcoming the rapid deactivation of the catalyst. Finally, the data presented in Fig.1 can be summarised in one sentence: non-PGM catalysts have a greater resistance to sulfur poisoning as well as being 3-4 orders of magnitude less expensive than PGM catalysts. These features make them ideal for the design of durable and economical residual methane abatement technologies [25].

In order to maximise the exposed surface area of a catalyst and minimise the backpressure of the after-treatment, catalysts are supported onto a substrate with a high surface area and low resistance to gas flow. Currently, cordierite monoliths with a honeycomb structure are the established technology, used mostly in internal combustion engine vehicles [26]. However, using this type of support implies an inevitable trade-off between catalytic performance and engine efficiency [25,27]. In contrast, using hollow fibre-based supports, which have a unique structure consisting of a variable number of parallel axial channels, bypasses this issue since the backpressure associated with these supports is an order of magnitude lower than that of state-of-the-art cordierite monoliths. In addition, the axial channels are surrounded by microscopic radial finger regions, which are responsible for their specific surface area to volume ratio being an order of magnitude larger than that of cordierite monoliths, allowing for larger catalyst loads. For these reasons, hollow fibre-based supports have proven to have the potential to be an excellent support for methane abatement catalysts [25,28].

Even though hollow fibre reactors have been studied as a suitable candidate for methane emission control technologies [25,27,29,30], it has not yet been proven that this technology is scalable and suitable for continuous real operation. By scalable it is meant that hollow fibre reactors can be combined into a larger structurally and mechanically all-encompassing unit composed of multiple hollow fibres bound together. This work aims to scale up the hollow fibre reactor and prove its suitability for the treatment of methane emissions arising from natural gas power plants (i.e. 1500 ppmV of methane), testing under extreme conditions (i.e. 100 ppmV of sulfur dioxide) and using realistic operating time frames (i.e. 1000 h). The technology studied in our previous work [25] has been chosen as a scalable unit to design and test a scaled-up hollow fibre after-treatment impregnated with an iron and chromium-based oxide catalyst (Fe:Cr 60:40). Two 7-fibre hollow fibre after-treatments composed of 7-channel fibres and 4-channel fibres, respectively, will be compared to assess the effect that the number of channels of the hollow fibre has on mass transfer and catalyst loading of the hollow fire reactor. Based upon the preliminary data gathered in the first stage of this study, the best performing hollow fibre after-treatment is going to be tested for a continuous 1000 h stability test (i.e. 40+ days) under extreme conditions including 100 ppmV of sulfur dioxide, a concentration up to 100 times larger than that present alongside residual methane emissions. Finally, 10 consecutive thermal shocks are going to be carried to test the thermal stability of this hollow fibre after-treatment.

## 2. Experimental

### 2.1. Synthesis of the hollow fibre bundle

The asymmetric 7-channel and 4-channel ceramic hollow fibres were synthesised through a combined phase-inversion and sintering technique. The spinning process was carried out by extruding the α-$Al_2O_3$ powder and polymer suspension through a seven-bore or four-bore spinneret, respectively, into an external coagulant. The hollow fibre precursors were left in the external coagulant overnight for complete solidification. After drying at room temperature, the fibres were sintered at high temperatures between 1350-1550 °C for 5 h. Further information can be found elsewhere [27,30,31]. The assembly of the 7-channel hollow fibre bundle and 4-channel hollow fibre bundle followed the same process. The respective hollow fibres were bound together using ceramic adhesive Ceramabond 503 (Aremco). The hollow fibres were first bound into a layer of 3 fibres and two

layers of 2 fibres and then the layers were bound together. The bundle was left to air dry for 1 h. The bundle was then step cured, under an air atmosphere, at 100 °C for 1.5 h, 250 °C for 1.5 h, 400 °C for 1.5 h and 600 °C for 1.5 h. The temperature ramp between each step was 20 °C/min and the time required to reach the following temperature was excluded from the 1.5 h step time.

## 2.2. Synthesis of the catalyst and impregnation of the hollow fibre bundle

Iron (III) nitrate nonahydrate (Sigma-Aldrich), chromium (III) nitrate nonahydrate (Sigma-Aldrich), citric acid monohydrate (Sigma-Aldrich) and anhydrous ethylene glycol (Sigma-Aldrich) were used to prepare a homogeneous catalyst solution following the sol-gel Pechini method [22]. The impregnation of the hollow fibre bundles consisted of a three-step procedure: i) impregnation of the hollow fibre bundles with the sol-gel solution, ii) drying in a ventilated oven (SciQuip Oven-55S) at 100 °C for 48 h, and iii) calcination under a 150 $mL \cdot min^{-1}$ air flow at 600 °C for 5 h. The catalyst deposition was calculated by measuring the difference in weight of the micro-structured unit before and after impregnation. Throughout the paper, the catalyst-impregnated 7-channel hollow fibre bundle and 4-channel hollow fibre bundle will be referred to as 7-channel after-treatment and 4-channel after-treatment. Finally, part of the catalyst solution was dried at 100 °C for 24 h and calcined at 600° C for 5 h to yield 2 g of powdered catalyst (i.e. Fe60Cr40) for XRD and XPS characterisation before and after the reaction.

## 2.3. Experimental apparatus and procedure

Information regarding the experimental apparatus used in this investigation can be found elsewhere [22]. The performance of the impregnated after-treatments for the total oxidation of methane was evaluated under four different reactant mixtures (BOC, steam added via a bubbler): i) dry conditions – 1500 ppmV of methane balanced in synthetic air, ii) wet conditions – 1458 ppmV of methane and 2.8%vol of steam balanced in synthetic air, iii) sulfur conditions – 1500 ppmV of methane and 100 ppmV of sulfur dioxide balanced in synthetic air and iv) extreme conditions - 1457 ppmV of methane, 2.8%vol of steam and 100 ppmV of sulfur dioxide balanced in synthetic air.

The after-treatments were loaded into the reactor and the reactions were carried over in the following order, consecutively: i) dry conditions - 10 h stability followed by light off, ii) wet conditions - 10 h stability followed by light off, iii) sulfur conditions - 10 h stability followed by light off and iv) extreme conditions - 10 h stability followed by light off. The 10 h stability tests were carried out at atmospheric pressure at a constant temperature of 550 °C under all reactant conditions. The light-off experiments were carried out at atmospheric pressure within the 25 to 600 °C temperature range under all reactant conditions.

In the case of the 4-channel after-treatment, a continuous 1000 h stability test under extreme conditions at 550 °C followed by 10 thermal shock experiments were carried over after the light-off under extreme conditions carried in the first stage of this study. During the thermal shock experiments, the hollow fibre after-treatment was heated using a ramp rate of 25 °C/min, reaching 550 °C in approximately 20 min. The methane reading for the thermal shock experiments under extreme conditions at atmospheric pressure were taken at 550 °C. Finally, 500 mg of powdered catalyst were aged under extreme conditions at 550 °C to obtain reacted catalyst for XRD and XPS characterisation.

For all experiments, the feed gas flowrate was 150 mL·min$^{-1}$. The effluent gas was monitored by in-line mass spectrometry (EcoSys-PTM Mass Spectrometer). The conversion of methane, X(%), was calculated using eq. 1:

$$X(\%) = \frac{[CH_4]_{in} - [CH_4]_{out}}{[CH_4]_{in}} \times 100 \qquad \text{(eq. 1)}$$

## 2.4. Characterisation of the hollow fibre after-treatment: scanning electron microscopy and energy-dispersive X-ray spectroscopy

The surface topography of the central fibre of the after-treatments was studied using a Zeiss Crossbeam 550 Scanning Electron Microscope (SEM). The samples were uncoated, the working distance was set to 5.2 mm, and the FIB probe voltage and current were 30 kV and 50 pA, respectively. The elemental composition of the 4-channel after-treatment was studied by Energy-dispersive X-ray Spectroscopy (EDX) mapping using an Oxford

Instruments X-Max 150 silicon drift detector, with an accelerating voltage of 15 kV and a beam current of 500 pA. EDX maps were collected for approximately 3 min until the signal to noise was sufficient.

## 2.5. Characterisation of the powdered Fe60Cr40 catalyst: powder X-ray diffraction and X-ray photoelectron spectroscopy

Fresh and reacted powdered Fe60Cr40 catalyst was analysed through XRD and XPS characterisation. The reacted catalyst was crushed and sieved to 125-250 μm using stainless-steel sieves (Fieldmaster). This catalyst was reacted under extreme conditions, at atmospheric pressure, at a temperature of 550 °C for a duration of 10 h.

X-ray diffraction (XRD) analysis was carried out to determine the crystal phase and crystallinity of powdered Fe60Cr40 catalyst. An X'Pert PRO Multipurpose Diffractometer (Panalytical) was used to record powder x-ray diffraction (XRD) patterns using Co K(α) irradiation (λ = 1.790307 Å), a step size of 0.02°, a 2θ range of 10°- 90° and a time step of 1.875°/min. The samples were placed in a silicon substrate zero-background sample holder. The obtained diffraction patterns have been analysed using X'Pert HighScore Plus software and compared to the ICDD database Powder Diffraction Files (PDF-3).

The surface chemical composition and surface element valence state of the powdered Fe60Cr40 catalyst was studied using an ESCALAB 250 X-ray photoelectron spectrometer (Thermo Fisher) equipped with an Al-Ka X-ray source. The bond energies were referenced to the adventitious C 1s line (284.6 eV).

## 3. Results and Discussion

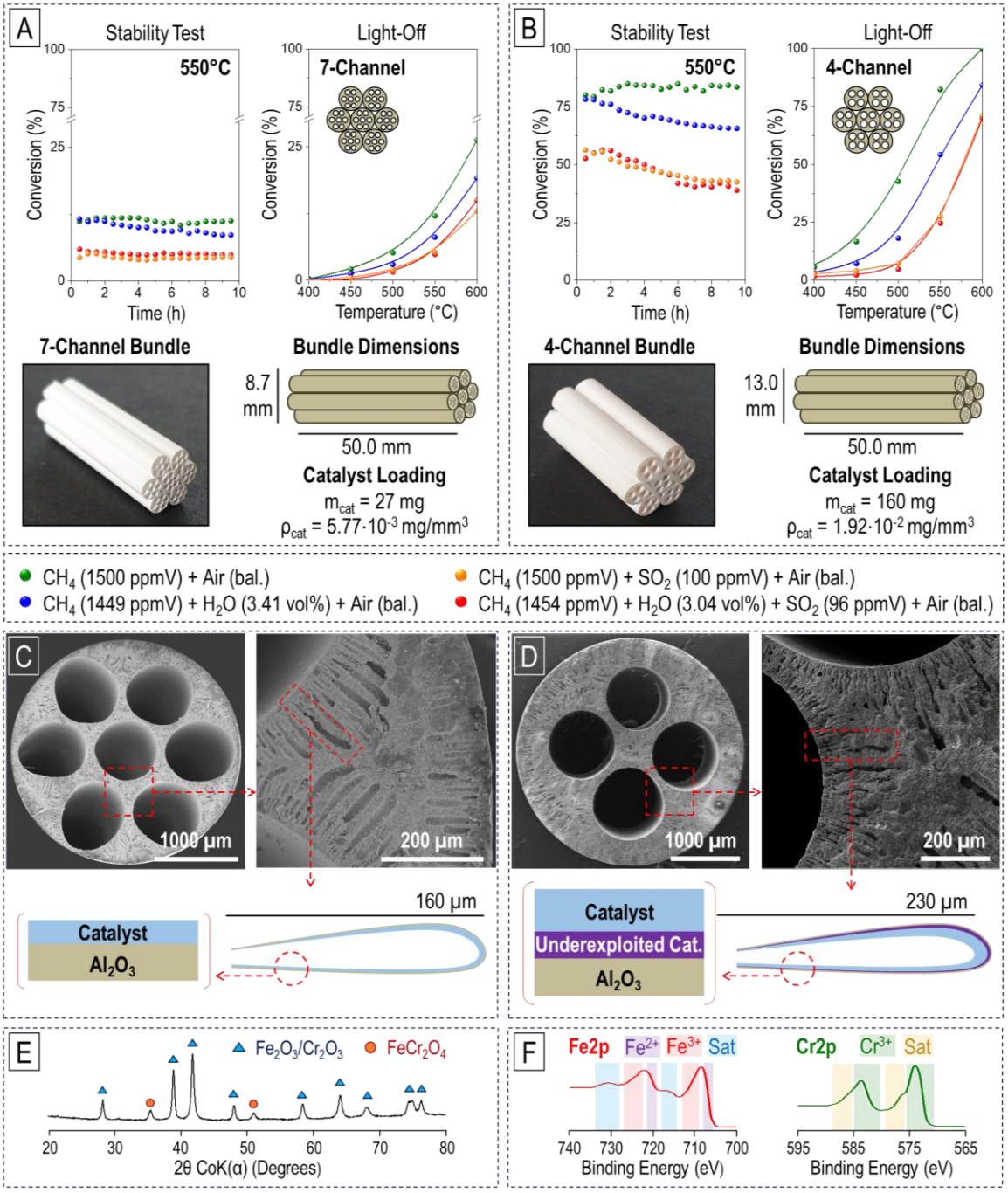


*Fig. 2: A) (clockwise) 7-channel bundle stability test, light-off after 10 h reaction, specifications and photograph; B) (clockwise) 4-channel bundle stability test, light-off after 10 h reaction, specifications and photograph; C) SEM images of the 7-channel after-treatment and graphical representation of the catalyst deposition inside the finger micro-channel; D) SEM images of the 4-channel after-treatment and graphical representation of the catalyst deposition inside the finger micro-channel; E) Fresh and aged XRD diffractogram of the powdered Fe60Cr40 catalyst impregnated into the hollow fibre bundle;*

*F) Fresh and aged XPS spectra of the Fe2p and Cr2p regions of the powdered Fe60Cr40 catalyst impregnated into the hollow fibre bundle.*

The stability and light-off tests of the 7-channel and 4-channel after-treatments can be found in Figs. 2A and 2B, respectively. At first sight, the same trends can be observed for both after-treatments. During the 10 h stability test, the methane conversion was hindered with the addition of steam and/or sulfur. In both cases, the methane conversion stayed constant throughout the 10 h under dry conditions and decreased under wet, sulfur and extreme conditions. As can be seen in Fig. 2A, the methane conversion under dry conditions of the 7-channel after-treatment had remained constant by the end of the 10 h. Whereas, under wet, sulfur and extreme conditions, the conversion had decreased by 26%, 14% and 18%, respectively. Similarly, Fig. 2B shows that, under dry conditions, the methane conversion of the 4-channel after-treatment had remained constant by the end of the test and had decreased by 16%, 24% and 26% under wet conditions, sulfur conditions and extreme conditions, respectively. Regarding the light-off tests, the light off curve was shifted towards higher temperatures for both after-treatments in the following order: dry conditions, wet conditions and, in a similar position, sulfur conditions and extreme conditions.

As previously mentioned, similar trends and behaviours have been observed for both after-treatments, which was expected since both after-treatments have been impregnated with the same catalysts, Fe60Cr40. However, on average, the methane conversions obtained for the stability study of the 4-channel after-treatment were 9 times larger than those obtained for the 7-channel after-treatment. Similarly, the light-off curves obtained for the 4-channel after-treatment all surpassed the light-off temperature (i.e. $T_{50}$) within the 500-600 °C temperature range. Whereas none of the light-off curves obtained for the 7-channel after-treatment surpassed the light-off temperature and the maximum methane conversion of 26% was achieved under dry conditions at 600 °C. This disparity in methane conversion levels can be explained by the fact that the catalyst loading of the 4-channel after-treatment was almost 6 times larger than that of the 7-channel. Taking into consideration the volume of the 7-channel after-treatment (i.e. 4677 $mm^3$) and the 4-channel after-treatment (i.e. 8314 $mm^3$), the catalyst loading density of these systems was calculated to be $5.77 \cdot 10^{-3}$ $mg/mm^3$ and $1.92 \cdot 10^{-2}$ $mg/mm^3$, respectively. Comparing these two values it can be realised that the catalyst impregnation process is more efficient when using 4-channel hollow fibres since the catalyst loading density of this system was 3.33 times larger than that of the 7-channel after-treatment.

The scanning electron microscopy images of the 7-channel and 4-channel after-treatments have been presented in Figs. 2C and 2D, respectively. As can be seen, the length of the finger micro-channels of the 4-channel after-treatment is 44% larger than those of the 7-channel, leading to a greater finger micro-channel volume. This explains the greater catalyst loading density of the 4-channel hollow after-treatment. However, even though the catalyst loading density of the 4-channel after-treatment is superior to that of the 7-channel after-treatment, the impregnated catalyst is used more efficiently in the 7-channel after-treatment. On average, the methane conversion rates shown in Figs. 2A and 2B, normalised per mass of catalyst, are 1/3 smaller for the 4-channel hollow after-treatment when compared to the 7-channel after-treatment. This suggests that in the 4-channel hollow after-treatment the catalyst is impregnated as a thin film, whereas in the 7-channel after-treatment the film is thicker, giving rise to an intermediate layer of underexploited catalyst, as shown in Figs. 2C and 2D. It is also possible that certain entry pores to the finger micro-channels could have been blocked due to an excessive catalyst load [29]. Nevertheless, since the used catalyst is inexpensive (2.64 $/Kg) and volume is the main constraint of the real application of this technology, a trade-off between a large catalyst loading density and a less efficient catalyst use is justified.

The same catalyst precursor that was impregnated into the hollow fibres was subjected to an identical calcination program to yield a powdered Fe60Cr40 catalyst, suitable for XRD and XPS characterisation. This catalyst was also reacted under extreme conditions for 10 h, as described in the experimental section. The XRD diffractogram of the Fe60Cr40 catalyst can be found in Fig. 2E. Note that the XRD diffractogram of the fresh and reacted catalyst was identical. As indicated in Fig. 2E, the diffraction peaks are characteristic of a solid solution of hematite and eskolaite [32]. In addition, two peaks at 35.12° and 50.6° indicate the presence of an iron (II) chromite spinel. Peaks attributable to iron sulfate or chromium sulfate were not observed, suggesting that the sulfates responsible for the catalyst's deactivation do not affect the bulk of the catalyst [22].

The Fe2p and Cr2p regions of the XPS spectra of the Fe60Cr40 catalyst have been presented in Fig. 2F. Similarly, the XPS spectra of the Fe60Cr40 catalyst was identical before and after the reaction. As highlighted, the Fe2p region shows peaks attributable to $Fe^{2+}$, $Fe^{3+}$ and the $Fe^{3+}$ satellites [33]. In the case of the Cr2p region, peaks attributable to $Cr^{3+}$ and its satellites can be observed [33]. There were no peaks attributable to sulfate chemical states observed in the S2p region [34].

In summary, the results obtained from the XRD and XPS characterisation are congruent, both supporting the presence of a dominant hematite and eskolaite solid solution with traces of an iron (II) chromite spinel. Similar results have been observed in our previous studies [22,25]. The obtained performance results indicate that sulfur dioxide is responsible for the irreversible deactivation of the catalyst impregnated into the after-treatments. However, these must be present in a concentration below the threshold of the detection limit of the equipment used.

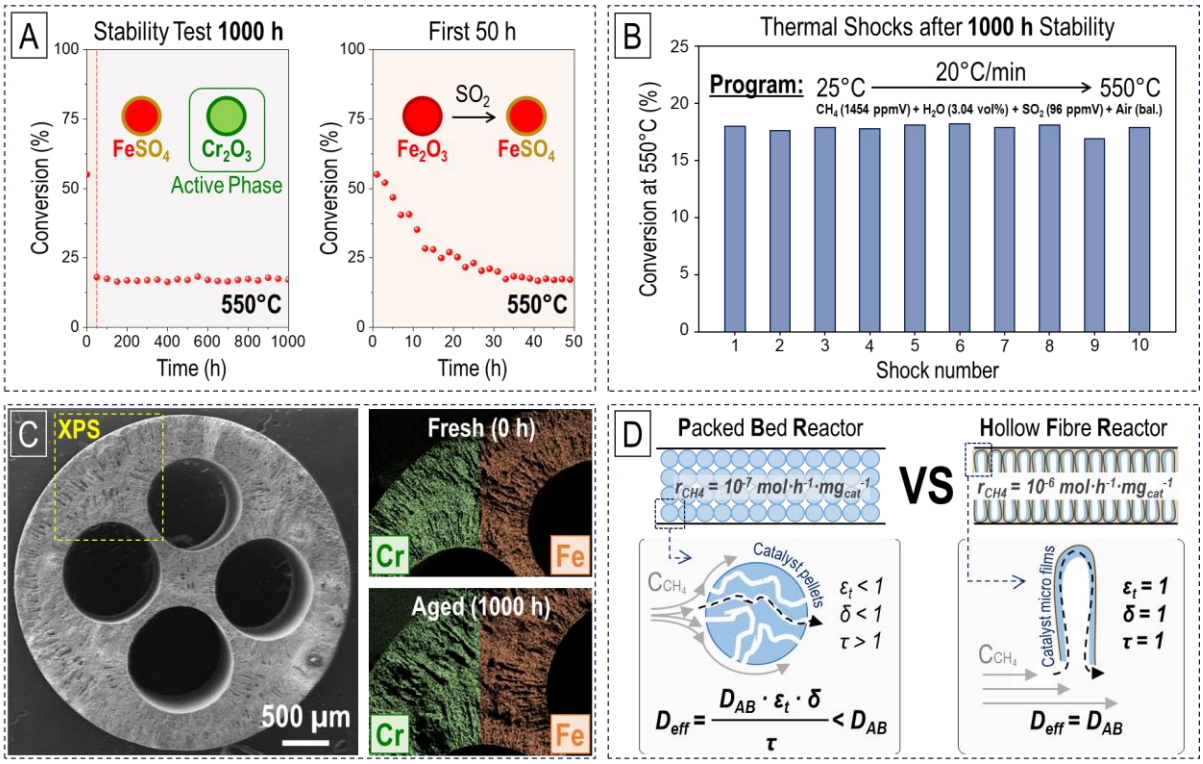


*Fig. 3: A) 4-channel bundle 1000 h long-term stability test; B) thermal shocks after 1000 h long-term stability test; C) SEM image and EDX map of the central hollow fibre of the 4-channel bundle; D) diffusion mechanisms in packed bed reactors and hollow fibre reactors.*

Due to its larger catalyst loading density, the 4-channel after-treatment was chosen for the 1000 h stability study shown in Fig. 3A and the thermal shock experiments shown in Fig. 3B. As can be seen in Fig. 3A, two trends can be observed; an initial deactivation period that lasted 33 h followed by a stable steady-state period until the completion of the experiment. The deactivation period can in itself be broken down into two stages, a rapid deactivation within the initial 15 h where the methane conversion dropped from 55% to 28% and a subsequent

slower deactivation from 28% to 17% in the 15 h to 33 h interval. From the 33rd hour of the experiment, the methane conversion of the after-treatment remained constant within the 16% to 18% range for the remaining 967 h of the experiment.

Previous works using both PGM and non-PGM catalysts agree that sulfur dioxide is responsible for the deactivation of methane emission control catalysts [8–10,13,15,23]. In the study presented herein, a concentration of 100 ppmV of sulfur dioxide has been used, a concentration which is 100 times higher than that present in emissions from natural gas power plants. As a result, during the 1000 h stability study, the after-treatment has been exposed to a total amount of sulfur dioxide superior to that of 11 years of continuous operation. Extreme levels of sulfur dioxide were used to accelerate the sulfur poisoning of the catalyst. It can be deduced that under real conditions, with sulfur dioxide levels within the 1 to 5 ppmV range, the deactivation of the catalyst would have been slower and each deactivation stage would have been observed over a proportionally longer timeframe.

As previously stated, the results obtained from the XRD characterisation of the Fe60Cr40 catalyst indicate it is a solid solution of hematite and eskolaite with traces of iron (II) chromite. Of these phases, hematite, which makes up around 60%wt of Fe60Cr40, is known to be irreversibly poisoned in the presence of sulfur dioxide. In contrast, eskolaite has previously proven to be stable under real conditions [15]. Furthermore, the initial conversion of 55% dropped by 2/3 before stabilising at 17%. Considering that approximately 2/3 of the catalysts' mass was hematite it is reasonable to state that the deactivation of the hematite phase is responsible for the overall deactivation of the catalyst. In our previous study [25], where the same catalyst was reacted for 10 h in the presence of 5 ppmV of sulfur dioxide, no signs of deactivation were observed. However, in the study presented herein, the sulfur dioxide concentration was 20 times larger and signs of deactivation were evident after the 5th hour on stream. In summary, the obtained results suggest that eskolaite is the phase responsible for most, if not all, the steady-state catalytic activity of the after-treatment during the 1000 h stability test.

Following the 1000 h stability study, the 4-channel after-treatment was subjected to thermal shock experiments. The thermal shock results have been presented in Fig. 3B. As can be seen, the methane conversion at 550 °C was within 16% and 18% for all 10 shocks. These methane conversion values are similar to those observed for the long-term stability test, as can be observed when comparing with the results shown in Fig. 3A. These results

indicate that the after-treatment is suitable for real operation including start-up and cool-down cycles. In addition, the results obtained from the EDX characterisation, shown in Fig. 3C, indicate that the catalyst remained homogeneously distributed after the 1000 h stability. This suggests that there was no catalyst peeling-off or sublimation during the experiment.

Finally, the diffusion mechanism of the reactant gases in a packed bed reactor and a hollow fibre reactor have been sketched and presented in Fig. 3D. As can be seen, in a traditional packed bed reactor, the granular structure of the catalyst gives rise to unavoidable gas flow obstacles quantified as porosity, constriction factor and tortuosity. These obstacles slow down the internal diffusion of the reactants, resulting in slower reaction kinetics. In contrast, using a hollow fibre as a catalyst support bypasses diffusion limitations, resulting in reaction kinetics that is as close to ideal kinetics as can be achieved. As a result, the observed kinetic constant is an order of magnitude larger than in a packed bed reactor [25].

## 4. Conclusion

The study presented herein has shown, for the first time, that (i) the hollow fibre reactor can be successfully scaled up, (ii) the number of channels of a hollow fibre impact its catalyst loading density, (iii) the scaled-up hollow fibre after-treatment is stable under extreme methane oxidation conditions and (iv) the catalyst impregnated into the hollow fibre after-treatments has excellent thermal stability.

In more detail, the comparison between a hollow-fibre after-treatment composed of 7-channel and 4-channel hollow fibres revealed the catalyst loading density of the 4-channel after-treatment was 3.33 times larger than that of the 7-channel after-treatment. However, the results indicate that the 4-channel after-treatment is mass transfer limited to some extent. Yet, since after-treatment volume is a key parameter when modifying natural gas turbines currently in operation and the used catalyst is inexpensive (2.64 $/Kg in June 2021), a trade-off between a large catalyst loading density and a less efficient catalyst use is justified.

Furthermore, the 4-channel after-treatment remained stable during the 1000 h stability study under extreme conditions including 100 ppmV of sulfur dioxide. After an initial deactivation period, the methane conversion levels remained stable at around 17% for the remaining 967 h of the experiment. Taking into consideration the

extreme sulfur dioxide concentration levels used in this experiment, it can be extrapolated that the after-treatment has been exposed to a total amount of sulfur dioxide superior to that of 11 years of continuous operation. In contrast, palladium-based catalysts get irreversibly poisoned within 1 h when 100 ppmV of sulfur dioxide are present alongside methane in the reactant feed [35]. In addition, thermal shocks are sparsely included alongside stability studies. In this study, the 4-channel after-treatment was subjected to 10 thermal shocks, which showed that the system has ideal thermal stability.

Note that the technology presented in this work can be scaled up to virtually any size, being able to treat residual methane emission volumes ranging from those of a household boiler to those of an 8,000 MW natural gas power plant. On a broader scale, the technology presented in this study has the potential to reduce annual methane emissions by 5.58 billion cubic metres, or about 2.15 times the water volume of Loch Lomond in Scotland. Taking into consideration the global warming potential of methane, each year these emissions will have the same global warming effect for the following 20 years as 180.29 billion cubic metres of carbon dioxide, a volume similar to twice the water volume of Lake Geneva in Switzerland. Therefore, regulating methane emissions must be a priority now that a suitable and inexpensive technology for eliminating methane emissions has been developed.

## 5. Author Contributions

**Miguel García-Vázquez** – Investigation (lead), Data Curation, Formal analysis, Writing - Original Draft, Writing - Review & Editing; **Pablo Marín** – Resources, Writing - Review & Editing, Supervision; **Salvador Ordóñez** – Resources, Writing - Review & Editing, Supervision; **Kang Li** – Resources, **Jinkun Tan** – Investigation (supporting), Resources; **Guangru Zhang** – Investigation (supporting), Resources and **Francisco R. García-García** – Conceptualization, Resources, Writing - Review & Editing, Supervision, Project administration, Funding acquisition.

## 6. Conflicts of Interest

There are no conflicts to declare.

## 7. Acknowledgements

This work was supported by the funding provided by The Carnegie Trust for the Universities of Scotland (grant RIG008664) and The University of Edinburgh Impact Acceleration Account (EPSRC grant J27318). Moreover, M. García-Vázquez gratefully acknowledges the funding provided by the School of Engineering at the University of Edinburgh to carry out his PhD.

## 8. References

[1] Natural Gas Information – Analysis - IEA, (n.d.). https://www.iea.org/reports/natural-gas-information-overview (accessed June 2, 2021).

[2] R.L. Siegelman, P.J. Milner, E.J. Kim, S.C. Weston, J.R. Long, Challenges and opportunities for adsorption-based CO2 capture from natural gas combined cycle emissions, Energy Environ. Sci. 12 (2019) 2161–2173. doi:10.1039/c9ee00505f.

[3] K. Tanaka, O. Cavalett, W.J. Collins, F. Cherubini, Asserting the climate benefits of the coal-to-gas shift across temporal and spatial scales, Nat. Clim. Chang. 9 (2019) 389–396. doi:10.1038/s41558-019-0457-1.

[4] R.K. Pachauri, L.A. Meyer, IPCC, 2014: Climate Change 2014: Synthesis Report. Contribution of Working Groups I, II and III to the Fifth Assessment Report of the Intergovernmental Panel on Climate Change, Geneva, Switzerland, 2014. http://www.ipcc.ch. (accessed November 22, 2018).

[5] T.N. Lavoie, P.B. Shepson, C.A. Gore, B.H. Stirm, R. Kaeser, B. Wulle, D. Lyon, J. Rudek, Assessing the Methane Emissions from Natural Gas-Fired Power Plants and Oil Refineries, Environ. Sci. Technol. 51 (2017) 3373–3381. doi:10.1021/acs.est.6b05531.

[6] M. Hoffmann, S. Kreft, G. Georgi, G. Fulda, M.M. Pohl, D. Seeburg, C. Berger-Karin, E. V. Kondratenko, S. Wohlrab, Improved catalytic methane combustion of Pd/CeO2 catalysts via porous glass integration, Appl. Catal. B Environ. 179 (2015) 313–320. doi:10.1016/j.apcatb.2015.05.028.

[7] H. Arandiyan, H. Dai, K. Ji, H. Sun, J. Li, Pt nanoparticles embedded in colloidal crystal template derived 3d ordered macroporous Ce0.6Zr0.3Y0.1O2: Highly efficient catalysts for methane combustion, ACS Catal. 5 (2015) 1781–1793. doi:10.1021/cs501773h.

[8] I. Friberg, N. Sadokhina, L. Olsson, The effect of Si/Al ratio of zeolite supported Pd for complete CH4 oxidation in the presence of water vapor and SO2, Appl. Catal. B Environ. 250 (2019) 117–131. doi:10.1016/j.apcatb.2019.03.005.

[9] N. Sadokhina, G. Smedler, U. Nylén, M. Olofsson, L. Olsson, Deceleration of SO2 poisoning on PtPd/Al2O3 catalyst during complete methane oxidation, Appl. Catal. B Environ. 236 (2018) 384–395. doi:10.1016/J.APCATB.2018.05.018.

[10] T. Lenk, A. Gärtner, K. Stöwe, T. Schwarz, C. Breuer, R. Kiemel, S. Casu, A High-Throughput Screening Approach to Identify New Active and Long-Term Stable Catalysts for Total Oxidation of Methane from Gas-Fueled Lean–Burn Engines, Catalysts. 10 (2020) 159. doi:10.3390/catal10020159.

[11] J. Lin, Y. Chen, X. Liu, X. Chen, Y. Zheng, F. Huang, Y. Xiao, Y. Zheng, L. Jiang, Microstructural property regulation and performance in methane combustion reaction of ordered mesoporous alumina supported palladium-cobalt bimetallic catalysts, Appl. Catal. B Environ. 263 (2020) 118269. doi:10.1016/j.apcatb.2019.118269.

[12] G. Zhao, X. Pan, Z. Zhang, Y. Liu, Y. Lu, A thin-felt Pd–MgO–Al2O3/Al-fiber catalyst for catalytic combustion of methane with resistance to water-vapor poisoning, J. Catal. 384 (2020) 122–135. doi:10.1016/j.jcat.2020.01.013.

[13] Y. Zhang, P. Glarborg, M.P. Andersson, K. Johansen, T.K. Torp, A.D. Jensen, J.M. Christensen, Sulfur poisoning and regeneration of Rh-ZSM-5 catalysts for total oxidation of methane, Appl. Catal. B Environ. 277 (2020) 119176. doi:10.1016/j.apcatb.2020.119176.

[14] Y. Ding, S. Wang, L. Zhang, L. Lv, D. Xu, W. Liu, S. Wang, Investigation of supported palladium catalysts for combustion of methane: The activation effect caused by SO2, Chem. Eng. J. 382 (2020) 122969. doi:10.1016/j.cej.2019.122969.

[15] S. Ordóñez, J.R. Paredes, F. V. Díez, Sulphur poisoning of transition metal oxides used as catalysts for methane combustion, Appl. Catal. A Gen. 341 (2008) 174–180. doi:10.1016/J.APCATA.2008.02.042.

[16] Q. Wang, Y. Peng, J. Fu, G.Z. Kyzas, S.M.R. Billah, S. An, Synthesis, characterization, and catalytic evaluation of Co3O4/γ-Al2O3 as methane combustion catalysts: Significance of Co species and the redox cycle, Appl. Catal. B Environ. 168–169 (2015) 42–50. doi:10.1016/j.apcatb.2014.12.016.

[17] F.F. Tao, J.J. Shan, L. Nguyen, Z. Wang, S. Zhang, L. Zhang, Z. Wu, W. Huang, S. Zeng, P. Hu, Understanding complete oxidation of methane on spinel oxides at a molecular level, Nat. Commun. 6 (2015) 1–10. doi:10.1038/ncomms8798.

[18] C. Liu, H. Xian, Z. Jiang, L. Wang, J. Zhang, L. Zheng, Y. Tan, X. Li, Insight into the improvement effect of the Ce doping into the SnO2 catalyst for the catalytic combustion of methane, Appl. Catal. B Environ. 176–177 (2015) 542–552. doi:10.1016/j.apcatb.2015.04.042.

[19] X. Wang, Y. Liu, Y. Zhang, T. Zhang, H. Chang, Y. Zhang, L. Jiang, Structural requirements of manganese oxides for methane oxidation: XAS spectroscopy and transition-state studies, Appl. Catal. B Environ. 229 (2018) 52–62. doi:10.1016/j.apcatb.2018.02.007.

[20] A. Choya, B. de Rivas, J.R. González-Velasco, J.I. Gutiérrez-Ortiz, R. López-Fonseca, Oxidation of residual methane from VNG vehicles over Co3O4-based catalysts: Comparison among bulk, Al2O3-supported and Ce-doped catalysts, Appl. Catal. B Environ. (2018). doi:10.1016/j.apcatb.2018.06.050.

[21] Q. Yu, C. Liu, X. Li, C. Wang, X. Wang, H. Cao, M. Zhao, G. Wu, W. Su, T. Ma, J. Zhang, H. Bao, J. Wang, B. Ding, M. He, Y. Yamauchi, X.S. Zhao, N-doping activated defective Co3O4 as an efficient catalyst for low-temperature methane oxidation, Appl. Catal. B Environ. 269 (2020) 118757. doi:10.1016/j.apcatb.2020.118757.

[22] M. García-Vázquez, K. Wang, J.M. González-Carballo, D. Brown, P. Landon, R. Tooze, F.R. García-García, Iron and chromium-based oxides for residual methane abatement under realistic conditions: A study on sulfur dioxide poisoning and steam-induced inhibition, Appl. Catal. B Environ. 277 (2020) 119139. doi:10.1016/J.APCATB.2020.119139.

[23] M. García-Vázquez, D. Satir, J.M. González-Carballo, P. Landon, R. Tooze, J. Tan, G. Zhang, F.R. García-García, The role of sulfur sinks and micro-structured supports on the performance of sulfur-sensitive non-PGM catalysts, Appl. Catal. A Gen. 622 (2021) 118201. doi:10.1016/j.apcata.2021.118201.

[24] Y. Guo, M. Wen, G. Li, T. An, Recent advances in VOC elimination by catalytic oxidation technology onto various nanoparticles catalysts: a critical review, Appl. Catal. B Environ. 281 (2021) 119447. doi:10.1016/J.APCATB.2020.119447.

[25] M. García-Vázquez, G. Zhang, Z. Hong, X. Gu, F.R. García-García, Micro-structured catalytic converter for residual methane emission abatement, Chem. Eng. J. 396 (2020) 125379. doi:10.1016/j.cej.2020.125379.

[26] X. Liu, J. Chen, G. Zhang, Y. Wu, P. Shen, L. Zhong, Y. Chen, Tuning the interactions among Ce, Pd and Rh over Ce-modified Pd-Rh three-way catalyst for exhaust treatment of natural gas vehicles, J. Environ. Chem. Eng. 9 (2021) 105570. doi:10.1016/J.JECE.2021.105570.

[27] N.I. Mahyon, T. Li, R. Martinez-Botas, Z. Wu, K. Li, A new hollow fibre catalytic converter design for sustainable automotive emissions control, Catal. Commun. 120 (2019) 86–90. doi:10.1016/J.CATCOM.2018.12.001.

[28] F.R. García-García, S.C. Tsang, K. Li, Hollow fibre based reactors for an enhanced H2 production by methanol steam reforming, J. Memb. Sci. 455 (2014) 92–102. doi:10.1016/j.memsci.2013.12.070.

[29] N.I. Mahyon, T. Li, B.D. Tantra, R. Martinez-Botas, Z. Wu, K. Li, Integrating Pd-doped perovskite catalysts with ceramic hollow fibre substrate for efficient CO oxidation, J. Environ. Chem. Eng. 8 (2020) 103897. doi:10.1016/j.jece.2020.103897.

[30] F.R. García-García, B.F.K. Kingsbury, M.A. Rahman, K. Li, Asymmetric ceramic hollow fibres applied in heterogeneous catalytic gas phase reactions, Catal. Today. 193 (2012) 20–30. doi:10.1016/J.CATTOD.2012.01.006.

[31] Z. Shi, Y. Zhang, C. Cai, C. Zhang, X. Gu, Preparation and characterization of α-Al2O3 hollow fiber membranes with four-channel configuration, Ceram. Int. 41 (2015) 1333–1339.

doi:10.1016/J.CERAMINT.2014.09.065.

[32] S. Musić, S. Popović, M. Ristić, Chemical and structural properties of the system Fe2O3-Cr2O3, J. Mater. Sci. 28 (1993) 632–638. doi:10.1007/BF01151237.

[33] M.C. Biesinger, B.P. Payne, A.P. Grosvenor, L.W.M. Lau, A.R. Gerson, R.S.C. Smart, Resolving surface chemical states in XPS analysis of first row transition metals, oxides and hydroxides: Cr, Mn, Fe, Co and Ni, Appl. Surf. Sci. 257 (2011) 2717–2730. doi:10.1016/J.APSUSC.2010.10.051.

[34] Y. Yan, P. Zhang, Z. Qu, M. Tong, S. Zhao, Z. Li, M. Liu, Z. Lin, Carbon/Sulfur Aerogel with Adequate Mesoporous Channels as Robust Polysulfide Confinement Matrix for Highly Stable Lithium–Sulfur Battery, Nano Lett. 20 (2020) 7662–7669. doi:10.1021/ACS.NANOLETT.0C03203.

[35] P. Gélin, M. Primet, Complete oxidation of methane at low temperature over noble metal based catalysts: a review, Appl. Catal. B Environ. 39 (2002) 1–37. doi:10.1016/S0926-3373(02)00076-0.